9498 *Macromolecules* **2009**, *42*, 9498–9505
DOI: 10.1021/ma901517z

Macromolecules
ARTICLE

Rotational and Conformational Dynamics of a Model Polymer Melt at Solid Interfaces

Michael Vogel*

Institut für Festkörperphysik, Technische Universität Darmstadt, Hochschulstrasse 6, 64289 Darmstadt, Germany

Received July 13, 2009; Revised Manuscript Received November 2, 2009

ABSTRACT: Performing molecular dynamics simulations for an all-atom model, we investigate the rotational and conformational dynamics of short poly(ethylene oxide) chains sandwiched between two parallel TiO_2 surfaces. In this nanocomposite, the polymer forms layers parallel to the solid interfaces. At the studied temperatures, a substantial slowdown of polymer dynamics with respect to the bulk behavior is essentially restricted to the layer next to the solid interface. While the rotational correlation times in the surface layer follow an Arrhenius law, non-Arrhenius behavior is found for segments in the center of the slit. Moreover, unlike bulk segments, interfacial segments show a jump diffusion mechanism. In the immediate vicinity of the solid surfaces, the waiting times between conformational transitions are longer and the probabilities for back jumps are higher, in harmony with the slower loss of orientational correlation in these regions. The transitions between the conformational states do not obey Poisson statistics, particularly in the layer next to the interface. At sufficiently low temperatures, correlated forward−backward motion is an important aspect of the conformational relaxation, leading to strongly nonexponential distributions for the waiting times of the dihedrals in the various conformational states.

I. Introduction

The dynamics of polymer melts near solid interfaces is of enormous interest for many technologically important phenomena such as adhesion, lubrication, coating, and wetting.[1] Moreover, polymer−solid interfaces largely determine the performance of polymer nanocomposites in new applications for biomaterials, sensors, and batteries. In general, the vicinity of solid interfaces strongly affects structure and dynamics of polymers. Therefore, in the quest of optimizing hybrid materials on polymer basis, it is of fundamental importance to understand the effects of solid interfaces on polymer behavior on an atomistic level. In addition, such insights can provide valuable information about a proposed equivalence between polymer nanocomposites and polymer thin films.[2−4]

A large number of experimental studies have improved our knowledge about the effects of solid interfaces on the dynamical behavior of polymer melts approaching their glass transition temperatures T_g. However, most experimental techniques lack spatial resolution so that important questions are still open.[5] On the one hand, changes of polymer dynamics can result because confinement imposes a length scale that possibly interferes with the length scale of cooperative dynamics. On the other hand, specific effects in the immediate vicinity of solid interfaces can be more important than the size of the confinement. If the latter is true, the question will arise whether the different dynamical behaviors result from direct polymer−surface interactions or from density variations near solid interfaces. To tackle these problems, it is necessary to determine the temperature-dependent range and relevance of surface-induced effects. Furthermore, for a fundamental understanding of polymer dynamics near inner surfaces, it is of particular importance to investigate how these surfaces affect the rate of conformational transitions, i.e., the intrinsic polymer dynamics.

MD simulations provide straightforward access to spatially resolved structure and dynamics of polymers in confined geometries and, hence, this method is a versatile tool to tackle the above questions. MD simulations of coarse-grained polymer models yielded valuable information about general aspects of polymer structure and dynamics near attractive and repulsive walls of various roughnesses.[6−10] These studies showed that interfaces, in particular attractive interfaces, engender density oscillations in a polymer melt. Moreover, attractive interactions were found to lead to a slowdown of polymer dynamics and to an increase of T_g, while repulsive surfaces were reported to result in an acceleration of polymer dynamics and a decrease of T_g.[6,7] Such coarse-grained polymer models neglect details of the intramolecular energetics, e.g., torsional barriers, which have been regarded as important for various kinds of relaxation processes in polymer materials.[11]

MD simulations of all-atom polymer nanocomposite models are more scarce since they became feasible only recently due to the rapid improvement of computer technology. Borodin et al.[12] showed that the conformational and structural relaxations of poly(ethylene oxide) (PEO) are substantially slower and more heterogeneous near TiO_2 surfaces than in the bulk. Kuppa et al.[13,14] found that polymer motion in clays is affected by not only the confinement, but also the presence of cations, leading to pronounced dynamical heterogeneities. Harmandaris et al.[15] reported a slowdown of conformational and structural polymer relaxation at a polyethylene/graphite interface, where the effects are anisotropic and restricted to the immediate vicinity of the inner surface. Likewise, Smith et al.[16] observed that the dynamics of poly(dimethylsiloxane) is slower near silica surfaces. Eslami and Müller-Plathe[17] demonstrated for polyamide confined between graphite surfaces that the rotational correlation times exhibit an oscillatory behavior as a function of the galley height with maxima corresponding to well-formed structures parallel to the surfaces. Moreover, the correlation times are longer close to the solid interfaces than in the center of the slit. Despite this recent progress, very little is still known about the temperature dependence of the interface effects, which does not only enable new

 Published on Web 11/18/2009

insights, e.g., by comparisons with experimental data, but can also be of importance for technological applications. Kuppa et al.[13,14] provided temperature-dependent information, but presence of ions leads to additional effects in their models.

Here, we perform MD simulations for an all-atom model of PEO−TiO_2 in a broad temperature range. For several reasons, we use the model developed by Borodin et al.[12] on the basis of quantum chemistry simulations. First, these workers established the reliability of the force-field on the basis of polymer structure and dynamics at a relatively high temperature $T = 423$ K, but they did not study the temperature dependence, which is the main focus of the present approach. Moreover, PEO nanocomposites were investigated in several experimental studies, e.g., in our recent ^{2}H NMR spectroscopy work,[18] so that we expect synergetic effects from combined experimental and computational efforts. Finally, we used the same PEO model in our previous MD simulation study[19] of the pure melt so that it is straightforward to monitor temperature-dependent effects of the TiO_2 surfaces in some detail. The PEO chains investigated in our recent and present simulation approaches are comprised of 12 monomers and capped by methoxy end groups. Such low-molecular weight materials do not only facilitate equilibration in simulation studies, but they were also used in a number of experimental works since they are regarded as promising candidates to improve the ionic conductivity of polymer electrolytes that do or do not contain nanoparticles.[20−24]

Conformational dynamics are of central importance for the structural relaxation of polymers.[11] For pure PEO melt, we observed that conformational dynamics cannot be described as a Markov process at sufficiently low temperatures, but correlated forward−backward jumps are an important aspect, which delay conformational and structural relaxations.[19] Therefore, the temperature-dependent interplay of conformational and structural relaxations close to solid interfaces is investigated in some detail in the present contribution.

II. Methods

The studied model contains 108 PEO oligomers sandwiched between 2 TiO_2 sheets. The oligomeric chains have the structure H−[CH_2−O−CH_2]$_{12}$−H. The TiO_2 sheets are parallel to the xy plane and each sheet is formed by 12 × 12 elementary units of anatase structure, leading to a dimension of 4.54 nm × 4.54 nm. The slit between the two inner TiO_2 surfaces has a width of about 4.4 nm, slightly depending on temperature. Altogether, the model contains 12744 atoms, 3456 in TiO_2 and 9288 in PEO. The well established quantum-chemistry based all-atom force field of Borodin et al.[12] was employed to describe the interatomic interactions.

We used the methodology that had been utilized in our previous simulation work on pure PEO.[19] Briefly, the MD simulations were performed with the GROMACS software package,[25] applying a time step of 1 fs. The nonbonded interactions were calculated utilizing a cutoff distance of 12 Å. The particle-mesh Ewald technique[26] and the LINCS algorithm[27] were employed to treat the Coulombic interactions and to constrain the bonds, respectively. Following Borodin et al.,[12] the atoms of the TiO_2 sheets were frozen. We use periodic boundary conditions so that the TiO_2 sheets are infinite in x and y directions while PEO and TiO_2 layers alternate in z direction. The thickness of the TiO_2 layers amounts to 19 Å, ensuring that the studied PEO layer weakly interacts with its periodic images. Prior to data acquisition, the system was equilibrated in simulations at constant N, P, and T, using the Berendsen barostat[28] and the Nosé-Hoover thermostat.[29] Employing the semiisotropic pressure coupling option of GROMACS, pressure was only applied along the z direction. These equilibration runs spanned 10 ns at the lower temperatures. The subsequent production runs were performed in the canonical ensemble, i.e., at constant N, V, and T, employing the Nosé-Hoover thermostat. The trajectories were saved every 0.5 ps for later analysis. This time interval is sufficiently small so as to resolve the vast majority of the conformational transitions, while the resulting amount of data is still reasonable. The method to identify conformational transitions was described in our previous study.[19] The simulation results provide no evidence for an onset of crystallization in the studied time and temperature ranges ($T = 300-500$ K).

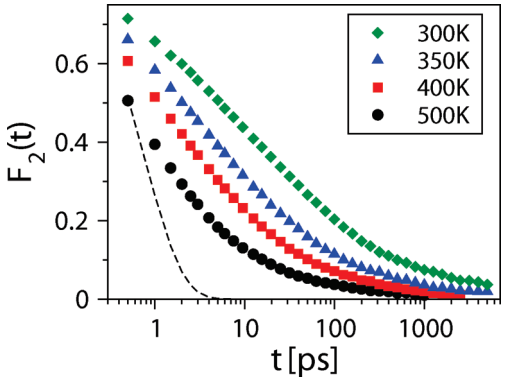

Figure 1. Temperature-dependent orientational correlation functions $F_2(t)$. For comparison, an exponential is shown as dashed line.

III. Results

A. Segmental Motion. First, we study temperature-dependent reorientation dynamics of the polymer segments in PEO−TiO_2. Specifically, we analyze the orientational autocorrelation function

$$F_2(t) = \frac{1}{2}\langle 3[\mathbf{e}(\tilde{t}_0 + t)\cdot\mathbf{e}(\tilde{t}_0)]^2 - 1\rangle \quad (1)$$

of C−H bonds in methylene gropus, i.e., we disregard the methyl end groups. Here, $\mathbf{e}(\tilde{t})$ is the unit vector describing the orientation of a C−H bond at a time $\tilde{t}$. Moreover, the brackets $\langle\ldots\rangle$ denote the averages over all C−H bonds in methylene groups and various time origins $\tilde{t}_0$. $F_2(t)$ is used to monitor PEO segmental rotational motion since it was measured in ^{2}H NMR stimulated-echo experiments on a PEO−TiO_2 nanocomposite.[18]

In Figure 1, we see that $F_2(t)$ shows strong nonexponentiality and pronounced temperature dependence. Use of a Kohlrausch−Williams−Watts (KWW) function does not enable satisfactory interpolation of the data since ca. 10% of orientational correlation are lost on relatively long time scales. Such long-time tail was not observed for pure PEO.[19] In view of the complex shape of the decays for PEO−TiO_2, we do not determine rotational correlation times τ from a fit of the decays, but from the criterion $F_2(\tau) = 1/e$. In Figure 2, it is evident that the temperature dependence of τ deviates from an Arrhenius law for both PEO and PEO−TiO_2. In our recent work on PEO,[19] we found that the slowdown of the dynamics is well described by a Vogel−Fulcher−Tammann (VFT) law

$$\tau(T) = \tau_\infty \exp\left(\frac{B}{T - T_0}\right) \quad (2)$$

For PEO−TiO_2, the temperature dependence is somewhat weaker, but still comparable. We cannot exclude that part of the difference results from the effect that the larger system size and the sluggish polymer dynamics close to the solid interfaces, see below, hamper complete equilibration of the nanocomposite at $T = 300$ K. Therefore, we refrain from quantifying the temperature dependence of τ for PEO−TiO_2.

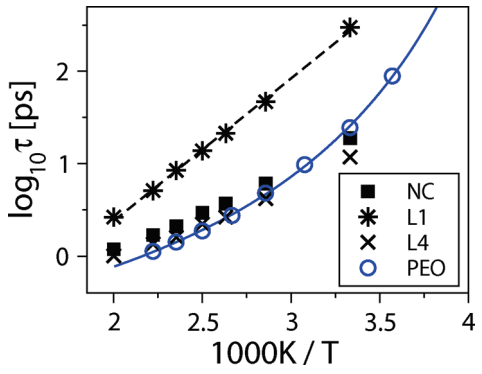

Figure 2. Temperature-dependent rotational correlation times τ for PEO−TiO_2 (NC) and PEO. The data for PEO was fitted to a Vogel-Fulcher law (solid line), yielding $T_0 = 191$K.[19] For PEO−TiO_2, we also separately study the correlation times of polymer dynamics in layers L1 and L4, respectively, see text for details. The results for layer L1 are interpolated with an Arrhenius law (dashed line), yielding an activation energy of $E_a = 0.31$ eV.

Borodin et al.[12] showed that PEO forms layers near the TiO_2 surfaces. Here, the existence of density oscillations is evident from the density profile of the carbon atoms perpendicular to the TiO_2 sheets, $\rho^C(z)$. In Figure 3a, we see that PEO is organized into three, or, possibly, four interfacial layers before bulk behavior is recovered. In these interfacial layers, which we denote as L1, L2, L3, and L4, in particular in L1, the carbon density exceeds the bulk density and, hence, polymer dynamics can depend on the distance from the nearest interface.[12] Therefore, we separately analyze the polymer dynamics in the various layers, i.e., we distinguish to which layer a carbon atom belongs at $t = 0$.

Figures 3(b) and (c) show orientational correlation functions $F_2(t; z)$, which separately characterize the polymer dynamics in the different layers. We see that segmental reorientation is significantly slower in L1 than in L4, in particular at low temperatures. Unlike $F_2(t)$, the orientational correlation functions of the respective layers, $F_2(t; z)$ do not exhibit a long-time tail. They are well described by a KWW function

$$A \exp\left[-\left(\frac{t}{\tau_K}\right)^{\beta_K}\right] \tag{3}$$

At 300 K, KWW fits yield $\tau_K = 11$ ps and $\beta_K = 0.34$ for L4 and $\tau_K = 296$ ps and $\beta_K = 0.20$ for L1, indicating slower and more stretched segmental relaxation near the solid interfaces. These results show that the long-time tail observed for the correlation function $F_2(t)$ of the whole ensemble stems from slow polymer segments in the immediate vicinity of the interfaces. The correlation times τ characterizing PEO dynamics in L1 and L4, respectively, are included in Figure 2. In the center of the slit, the values of τ are comparable to that of the bulk material. By contrast, in the interfacial layer, PEO dynamics is much slower and exhibits a stronger temperature dependence, at least at the studied temperatures. Specifically, τ of L1 follows an Arrhenius law with an activation energy of $E_a = 0.31$ eV rather than a VFT law.

This difference in the temperature dependence gives rise to the question whether the mechanism of PEO dynamics changes in the vicinity of the TiO_2 surfaces. To address this question, we calculate the van Hove self-correlation functions for the carbons and oxygens of PEO

$$G_X(\mathbf{r}; t) = \langle \delta[\mathbf{r_i}(\tilde{t}_0 + t) - \mathbf{r_i}(\tilde{t}_0) - \mathbf{r}] \rangle \tag{4}$$

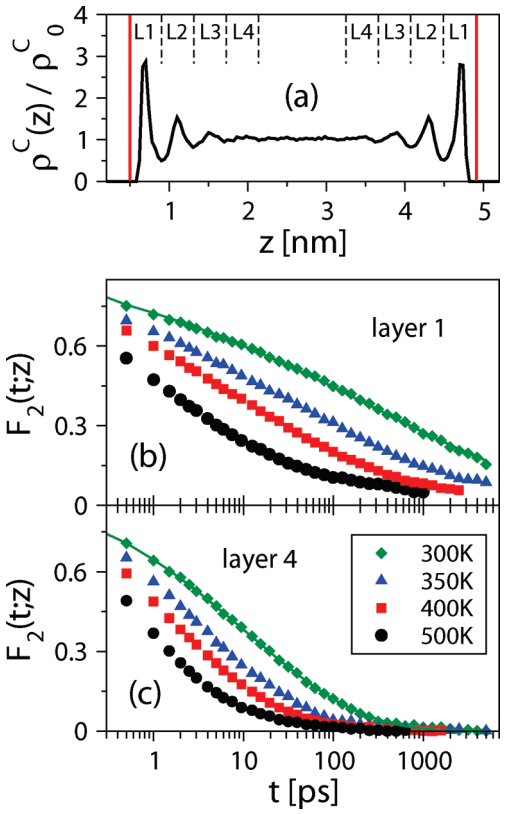

Figure 3. (a) Density profile along the z direction, i.e., perpendicular to the solid interfaces. We show the number density of the carbon atoms $\rho^C(z)$ at $T = 425$ K normalized by the bulk value, ρ_0^C. The solid vertical lines mark the surfaces of the TiO_2 sheets. The polymer forms layers parallel to the solid interfaces, which are denoted as L1, L2, L3, and L4. The thickness of all layers is $\Delta z = 0.50$ nm, corresponding to the distance between two consecutive minima of the density profile. Moreover, temperature-dependent orientational correlation functions $F_2(t;z)$ are displayed, which characterize polymer dynamics in different layers: (b) L1 and (c) L4. In both these panels, the solid lines are KWW fits to the data at $T = 300$ K.

Here, $\mathbf{r_i}(\tilde{t})$ denotes the atomic position at time $\tilde{t}$ and X = C, O. For isotropic samples, $4\pi r^2 G_X(r; t)$ measures the probability that an atom of the respective type moves a distance $r \equiv |\mathbf{r}|$ in a time interval t. In our case, anisotropy is imposed by the inorganic interfaces, but the effect does not alter our qualitative discussion. In the following, we again distinguish between different layers. Specifically, we compare $4\pi r^2 G_X(r; t = 5\text{ ns}, z)$ of layers L1 and L4 at $T = 300$ K in Figure 4. We see that, on average, the atomic displacements are larger for atoms that belong to L4 at the beginning of the studied time interval than for those that start from L1. Hence, like rotational motion, translational motion is slowed down for segments close to the TiO_2 surfaces. Moreover, it is evident that the shape of $G_X(r; t, z)$ resembles a Gaussian in the center of the slit, as expected for simple dynamics, while the Gaussian approximation is not obeyed in the vicinity of the solid interface. Specifically, a pronounced secondary maximum indicates that jump motion prevails in L1. The secondary maximum and thus, the jump length, ranges from about 3.0 to 3.6 Å for both oxygen and carbon atoms. For L4, such a second peak is not observed for shorter time intervals t either.

It is interesting to compare the jump length in L1 with various length scales characterizing the structure of PEO−TiO_2. In Figure 4a, we see that the density profile $\rho^O(x)$ of interfacial PEO oscillates parallel to the solid interfaces, where the length scale of the fluctuations is determined by

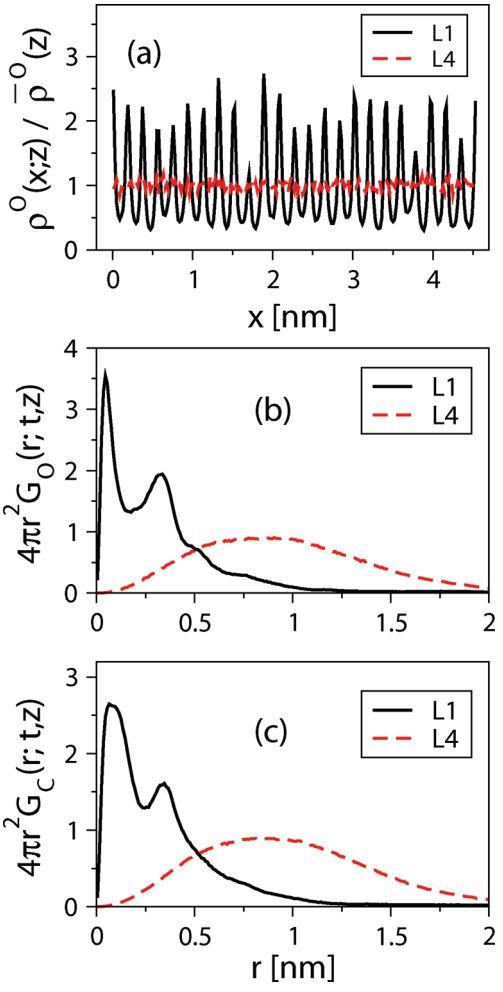

Figure 4. Results for PEO−TiO_2 at 300 K: (a) Density profiles along the x direction, i.e., parallel to the solid interfaces. We show the number density of the oxygen atoms $\rho^O(x; z)$ in layers L1 and L4 normalized by the average value $\bar{\rho}^O(z)$ in the respective layer. In panels b and c, we display the van Hove self-correlation functions $4\pi r^2 G_{C,O}(r; t,z)$ for the oxygen and carbon atoms of PEO, respectively, to separately analyze polymer translational motion in layers L1 and L4. A time interval $t = 5$ ns is considered.

the TiO_2 structure and amounts to 1.9 Å along the corresponding crystal axis. This value is much smaller than the jump length, providing evidence against the conjecture of Borodin et al.[12] who concluded that the PEO backbone atoms show vibrational motion in potential wells on the TiO_2 surface that is occasionally interrupted by jumps to the closest potential well. Furthermore, the observed jump lengths of 3.0−3.6 Å are smaller than the intermolecular interatomic distances of the backbone atoms, which are in the range of 4.5−6.0 Å. On the other hand, the jump length are consistent with the intramolecular oxygen−oxygen distances, implying that the atoms tend to replace equivalent atoms in the neighboring monomers along the polymer chain.

B. Conformational Dynamics. In the following, we investigate the torsional motion of PEO by analyzing trajectories of dihedral angles, $\phi(\tilde{t})$. For pure PEO, we found that the time evolution of the dihedral angles can be decomposed into long periods of librational motion within the *gauche*$^-$ (g^-), *trans* (t), or *gauche*$^+$ (g^+) states, which are interrupted by occasional transitions between the conformational states.[19] Because of the existence of well-defined jumps, mapping the continuous angular trajectories $\phi(\tilde{t})$ onto discrete sequences

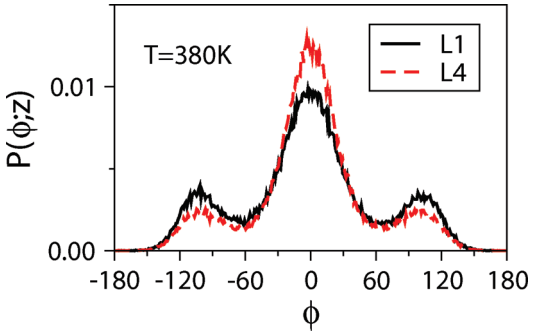

Figure 5. Probability distribution $P(\Phi; z)$ of the COCC dihedral angle describing the conformations in layers L1 and L4 at $T = 380$ K, respectively.

of the visited conformational states proved a very useful concept to eliminate effects from librational motions, which do not result in conformational relaxation. Specifically, this discretization allowed us detailed characterization of the relevant torsional motion in terms of waiting times t_w within the states and back-jump probabilities p_b between the states. Here, we exploit the capabilities of this approach to study effects of solid interfaces on the conformational dynamics of the PEO model. We focus on the COCC dihedrals, but we determined that qualitatively similar results are obtained for the OCCO dihedrals, consistent with our findings for pure PEO.[19] In Figure 5, the probability distribution of the COCC dihedral angle $P(\Phi; z)$ is compared for L1 and L4 at $T = 380$ K. We see that the t state is more probable than the $g^{\pm}$ states, but the difference is smaller for the interfacial layer.

First, we analyze the waiting times t_w in the conformational states, i.e., the time intervals between two subsequent conformational transitions. Valuable insights into the nature of the conformational dynamics are available from the probability distributions of the waiting times $p(t_w)$. Since waiting times, in general, depend on the dihedral species (OCCO/COCC) and the conformational state, we separately determine $p(t_w)$ for each species and state. Figure 6a shows the distribution $p(t_w^t)$, characterizing the waiting times of the COCC dihedrals in the t state. At short times, there are substantial deviations from an exponential waiting-time distribution, in particular at lower temperatures, indicating that a Markov process does not apply to the conformational dynamics. At long times, the decay is nearly exponential and more temperature dependent. Qualitatively similar waiting-time distributions are observed for the other dihedral species and conformational states. These findings imply that different contributions govern the distributions at short and long times, respectively.

The origins of the short-time and long-time contributions to $p(t_w)$ can be unraveled when we distinguish between forward and backward jumps.[19] Let $\sigma_{i-1} \rightarrow \sigma_i \rightarrow \sigma_{i+1}$ be a sequence of three subsequently visited conformational states ($\sigma_i = g^-, t, g^+$). Then, $\sigma_{i-1} \neq \sigma_{i+1}$ and $\sigma_{i-1} = \sigma_{i+1}$ result from a forward jump and a backward jump in the state σ_i, respectively. We focus on the jump direction in the t state since the behavior in this state is of particular importance for conformational relaxation due to the rareness of transitions $g^{\pm} \rightarrow g^{\mp}$ at sufficiently low temperatures. Specifically, unlike backward jumps, forward jumps in the t state enable exploration of all conformational states, as required for complete relaxation. Figure 6b shows the probability distributions $p(t_w^t)$ characterizing the waiting times in the t state during forward ($g^{\pm} \rightarrow t \rightarrow g^{\mp}$) and backward ($g^{\pm} \rightarrow t \rightarrow g^{\pm}$) sequences, respectively. We see that the shape of the waiting time distribution strongly depends on the jump

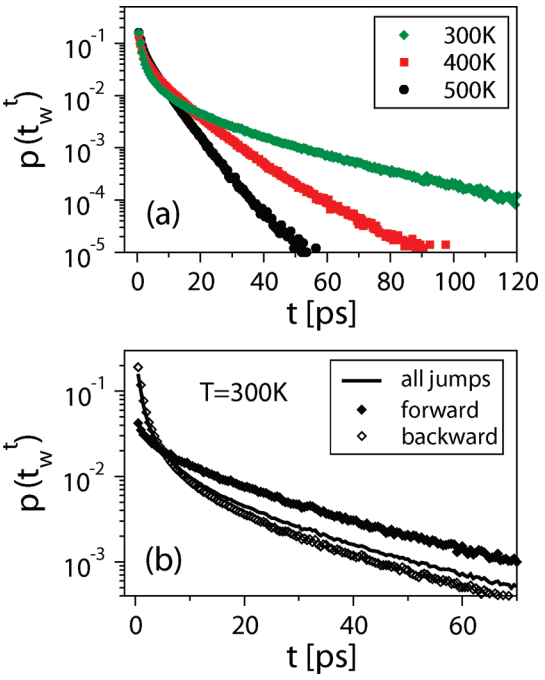

Figure 6. (a) Probability distributions $p(t_w^t)$ characterizing the waiting times of the COCC dihedrals in the t state at various temperatures. (b) Comparison of contributions to $p(t_w^t)$ resulting from forward jumps ($g^{\pm} \rightarrow t \rightarrow g^{\mp}$) and backward jumps ($g^{\pm} \rightarrow t \rightarrow g^{\pm}$), respectively. Data at $T = 300$ K are shown.

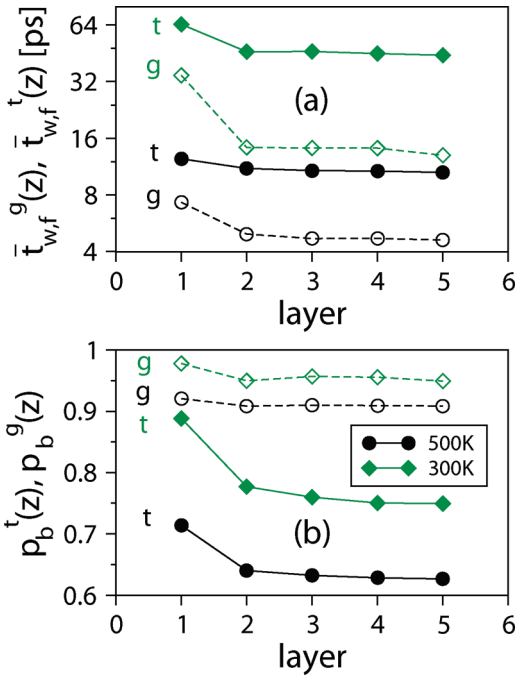

Figure 7. Comparison of conformational dynamics in different layers, i.e., as a function of the distance from the nearest solid interface: (a) Mean waiting times of the COCC dihedrals prior to forward jumps. We distinguish mean waiting periods in the t state, $\bar{t}^t_{w,f}(z)$, from that in the $g^{\pm}$ states, $\bar{t}^g_{w,f}$. (b) Back-jump probabilities $p^t_b(z)$ and $p^g_b(z)$. The former quantity is the probability that a jump $g^{\pm} \rightarrow t$ is followed by a direct backward jump $t \rightarrow g^{\pm}$; the latter is the probability that a jump $t \rightarrow g^{\pm}$ is followed by a direct backward jump $g^{\pm} \rightarrow t$. In both panels, we show results for $T = 300$ K (diamonds) and $T = 500$ K (circles).

direction. The deviations from exponential behavior are much stronger for backward jumps than for forward jumps. Hence, in the case of forward jumps, the propensity to perform a transition hardly depends on the jump history. In the case of the backward jumps, an enhanced probability at short times indicates correlated jump events. For pure PEO, we demonstrated that this nonexponentiality of the waiting time distributions results from correlated back jumps to a temporarily preferred conformational state,[19] see below.

Next, the conformational dynamics are characterized as a function of the distance from the nearest interface. In Figure 7a, we display spatially resolved mean waiting times prior to forward jumps in the t and $g^{\pm}$ states, $\bar{t}^t_{w,f}$ and $\bar{t}^g_{w,f}$, respectively. We focus on forward jumps since they are the cornerstone of conformational relaxation. First, it is evident that, for all conformational states and layers, the waiting times increase when the temperature is reduced from 500 to 300 K. However, the differences are moderate and, for all layers, they are substantially smaller than that of the respective correlation time τ, see Figure 2. Specifically, for L1, τ and $\bar{t}^t_{w,f}$ increase by factors of 112 and 5.2, respectively, when the temperature is decreased from 500 to 300 K.

Moreover, we see in Figure 7a that the dihedrals in L1 exhibit longer mean waiting times than that in the other layers. The effect is more pronounced for the $g^{\pm}$ states and at lower temperatures, but it is too small to explain the discrepancy of the rotational correlation times in L1 and L4, see Figure 2. In detail, at 300 K, τ is a factor of 25 longer in L1 than in L4, while $\bar{t}^g_{w,f}$ differs by only a factor of 2.4 between these layers. The finding that, at the TiO_2 surface, the increase of $\bar{t}^g_{w,f}$ is stronger than that of $\bar{t}^t_{w,f}$ can be rationalized when we reinspect Figure 5. We see that the fraction of dihedrals in the $g^{\pm}$ states is higher in L1 than in L4, indicating that the energy difference between the $g^{\pm}$ states and the t state is smaller at the solid interface. This decrease of the potential energy of the $g^{\pm}$ states relative to that of the t state results in a stronger increase of the waiting times in the former states than in the later state when approaching the TiO_2 surface, consistent with our findings in Figure 7a. Finally, the result that L2 exhibits mean waiting times that are already close to the bulk values indicates that the effect of the solid interface is rather short ranged. Consistently, we observe that F_2 of L2 (not shown) already resembles that of L4, see Figure 3b.

These findings imply that, for an understanding of the relaxation behavior, it is not sufficient to study single conformational transitions, but it is necessary to correlate the times and the directions of two or more events. First, we characterize the directions of two consecutive conformational transitions. For this purpose, we determine the back-jump probabilities p_b. The probability p^t_b that a transition $g^{\pm} \rightarrow t$ is directly followed by a transition $t \rightarrow g^{\pm}$ is presented in Figure 7b. We see that p^t_b is significantly higher in L1 than in the other layers, adding to a delay of conformational relaxation near the TiO_2 sheets. Also with respect to this aspect, the behavior of segments in L2 resembles that of the bulk material. The back-jump probability in the $g^{\pm}$ states, p^g_b, is significantly higher than p^t_b, reflecting the rareness of direct $g^{\pm} \rightarrow g^{\mp}$ transitions. This rareness is a consequence of the fact that the *cis* state, which separates the g^- and g^+ states, is energetically highly unfavorable, as can be inferred from the very low values of $P(\Phi)$ in the region $\Phi \approx \pm 180°$, see Figure 5. Unlike p^t_b, p^g_b only weakly depends on the distance from the nearest solid interface. In addition, we see that all back-jump probabilities substantially increase with decreasing temperature and, hence, back jumps are an important aspect of conformational relaxation at sufficiently low temperatures.

So far, we have shown that vicinity of a TiO_2 interface leads to longer waiting times and higher back-jump

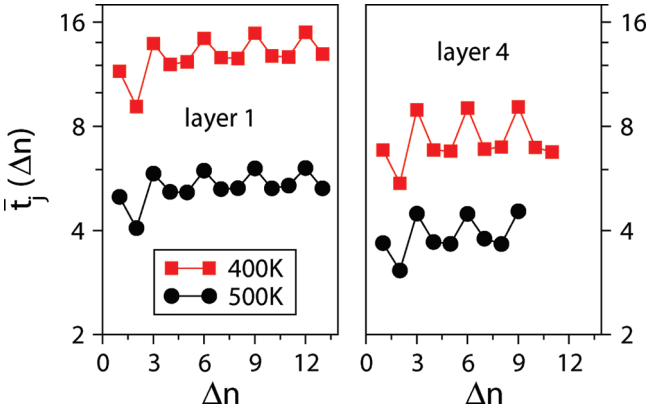

Figure 8. Mean time $\bar{t}_j(\Delta n; z)$ elapsing between the jump of an OCCO dihedral and the subsequent jump of another COCC or OCCO dihedral, which has a distance of Δn dihedrals along the backbone. The left and right panels show results from dihedrals in L1 and L4, respectively.

probabilities during PEO conformational relaxation. Now, the chronology of conformational transitions along the PEO chains is analyzed. For this purpose, we determine the mean times $\bar{t}_j$ elapsing between the conformational transition of a specific OCCO dihedral and the next conformational transition of each of the other dihedrals (COCC or OCCO) of the same chain. Figure 8 shows the mean times $\bar{t}_j$ as a function of Δn, being the difference of the indices of the initially and subsequently jumping dihedrals along the chain. When calculating these mean values, we distinguish between conformational dynamics in different layers. In detail, we only consider those contributions for which all main-chain atoms between the initially and subsequently jumping dihedrals belong to the same layer and we restrict ourselves to dihedrals in the centers of the chains so as to avoid effects from chain ends. For L1 and L4, $\bar{t}_j$ weakly depends on Δn. The observed pattern of $\bar{t}_j(\Delta n; z)$ mainly reflects the fact that the conformation dynamics of the COCC dihedrals is somewhat faster than that of the OCCO dihedrals and that pairs of the former dihedrals are separated by one of the latter dihedrals along the chains. A significantly smaller value of $\bar{t}_j$ is only observed for $\Delta n = 2$, i.e., for those dihedrals that share exactly one C−O bond. Such effect was also found in previous simulation studies on polymer melts and attributed to crankshaft motion.[30,31] Except for this crankshaft motion, our results show that the jump of one dihedral hardly triggers the jump of a specific neighboring dihedral along the chain, irrespective of the distance from the nearest solid interface.

Finally, we investigate the conformational dynamics of the COCC dihedrals on a longer time scale $t = 100$ ps $\approx 20\bar{t}_w$, where $\bar{t}_w$ is the mean waiting time of the COCC dihedrals regardless of the state. Specifically, we determine the probability distribution $P(n; t,z)$ of finding n conformational transitions during the time interval t. In Figure 9, we display the distributions $P(n; t,z)$ for L1 and L4 at $T = 400$ K. For both layers, there are pronounced deviations from a Poisson distribution, indicating that conformational dynamics do not conform to random statistics. Comparison of the data for L1 and L4 shows that the deviations from the Poisson distribution are more pronounced in the immediate vicinity of a solid interface. Specifically, $P(n; t,z)$ is much broader for L1, indicating that a large fraction of dihedrals performs either less or more transitions than expected for the case of uncorrelated jump events. Thus, the TiO_2 sheets lead to additional dynamical heterogeneity of the conformational dynamics, consistent with more stretched orientational correlation functions for interfacial PEO; see Figure 3.

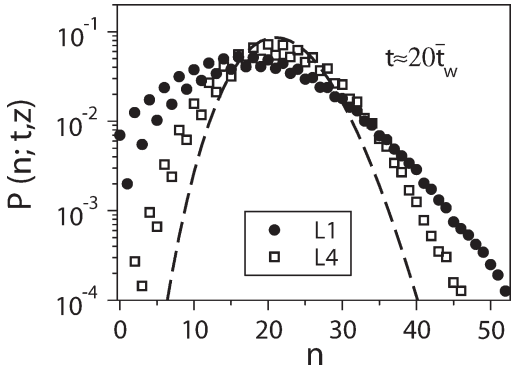

Figure 9. Probability $P(n; t,z)$ of finding n conformational transitions of a COCC dihedral during a time interval t at $T = 400$ K. We distinguish between dihedrals belonging to layers L1 and L4 at the beginning of the time interval,respectively. A time interval $t = 100$ ps $\approx 20\bar{t}_w$ is used. The dashed line is the Poisson distribution for the actual ratio $t/\bar{t}_w(z)$ in L4.

Furthermore, it is evident from Figure 9 that it is more probable to find an even than an uneven number of conformational transitions in a given time interval for sufficiently small values of n. This effect indicates the existence of correlated forward−backward jumps. It implies that, at a given time, each COCC dihedral has a preferred conformational state. After the exit of its preferred state, a dihedral tends to return to this state within a very short period of time performing a correlated backward jump. As a consequence, the dihedrals, on average, spend much longer times in the preferred state than in the other states, resulting in a higher probability of finding an even number of jumps, consistent with the observations in Figure 9. At $T = 400$ K, the difference between even and uneven n becomes small for $n > 35$, implying that the memory of the preferred state is lost after about 35 torsional jumps. With respect to this phenomenon, conformational dynamics hardly differ in L1 and L4. The time interval $t = 100$ ps used in the present analysis corresponds to the late stages of the loss of orientational correlation, see Figure 3, implying that the dihedrals remember their preferred state at least for large parts of the structural relaxation. In MD simulation work on a pure poly(butadiene) melt,[32] it was reported that the "homogenization time" of torsional motion, i.e., the time scale on which the heterogeneous nature and the self-correlations of conformational dynamics disappear, is strongly tied to the structural relaxation time.

C. Conclusions. Performing MD simulations for an all-atom model,[12] we have found that presence of TiO_2 strongly affects structure and dynamics of PEO. In the studied model, PEO is organized into layers parallel to two TiO_2 sheets, consistent with density oscillations previously reported for chemically realistic and coarse grained polymer models close to solid interfaces.[6−17] To determine the range of interface effects, we have separately ascertained the polymer dynamics in the different layers. The analysis has shown that PEO exhibits substantially slower rotational and translational dynamics close to the solid interfaces than in the center of the slit, in harmony with the outcome of previous simulation works on the dynamics of chemically realistic polymer models in the vicinity of solid interfaces.[12,15−17] However, at the studied temperatures, the slowdown is restricted to the layer next to the TiO_2 sheets; i.e., it is short ranged, implying that the changes of PEO dynamics are dominated by interface effects rather than confinement effects, restricting the length scale of cooperative dynamics.

Interestingly, we have found that the rotational correlation times of interfacial PEO and bulk PEO exhibit

Arrhenius and VFT temperature dependence, respectively. In view of this difference, one may conclude that cooperative dynamics of polymer melts are suppressed by attractive solid interfaces. Consistently, we have observed that, in the surface layer, a jump motion prevails, which involves jump lengths that do not correspond to intermolecular, but rather to intramolecular interatomic distances, specifically, to the typical distances between equivalent atoms in neighboring monomers along the backbone. The different temperature dependence of interfacial and bulk polymer dynamics may have intriguing consequences. When we speculate that the Arrhenius and VFT behaviors observed in the admittedly narrow temperature range of the present study can be extrapolated to much lower temperatures, the resulting curves $\tau(T)$ will intersect when approaching T_g. If this is true, highly viscous PEO will show comparable or even faster dynamics close to TiO_2 surfaces than in the bulk. Evidence for an enhancement of polymer dynamics close to solid interfaces comes from experimental studies in the vicinity of the glass transition. For PEO intercalated within a layered silicate, dielectric spectroscopy work observed a relaxation process α' between the bulk α and β processes.[33] The α' relaxation exhibits Arrhenius temperature dependence and stems from PEO in the immediate vicinity of the silicate layers. Likewise, for bulk PEO, a relaxation at intermediate times between structural and local relaxations was reported and attributed to polymer segments at the transition between crystalline and amorphous regions.[34] No clear evidence for bimodal polymer dynamics was found in our ^{2}H NMR study of PEO−TiO_2.[18] However, one should be very careful when comparing the results of these experimental approaches with that of the present work, because the former studied lower temperatures and higher molecular weights (M_w = 2000−100000). Nevertheless, it may be very important to take into account the respective temperature ranges when comparing effects of solid interfaces on the rates of polymer dynamics.

Characterizing the conformational dynamics of PEO in the vicinity of TiO_2, we have found that effects of the solid interfaces are restricted to the surface layer at the studied temperatures, consistent with our results for the segmental reorientation. For interfacial PEO, longer waiting times between conformational transitions and higher probabilities for back jumps to the previous conformational state contribute to the observed slowdown of orientational and translational motion with respect to the bulk behavior. However, these effects are not sufficient to explain the much longer rotational correlation times in the surface layer. Likewise, MD simulation studies on bulk polymers reported that the temperature dependence of the mean waiting times is weaker than that of translational and rotational correlation times, indicating that the longer waiting times in the conformational states are not sufficient to explain the strong slowdown of the structural relaxation upon cooling.[19,11,32] Moreover, studying the chronology of conformational transitions along individual chains, we found no evidence that, for interfacial or bulk PEO, the transition of one dihedral substantially triggers the transition of a specific neighboring dihedral along the chain, except for the known effect of crankshaft motion.[30,31]

These findings show that the structural relaxation in polymer melts cannot be understood on the basis of one or two conformational transitions, but it is important to follow the conformational dynamics for longer times. Therefore, we have analyzed the probability $p(n; t,z)$ of finding n conformational transitions during a time interval t, which was chosen such that, on average, ca. 20 transitions occur. The observed probability distributions $p(n; t,z)$ substantially deviate from a Poisson distribution, where deviations are stronger for interfacial PEO than for bulk PEO, in harmony with results in previous work on the studied model.[12] In particular, the actual distributions are broader than the corresponding Poisson distributions, and thus, the conformational dynamics are heterogeneous so that some of the dihedrals perform less or more transtions as compared to a Poisson process. The heterogeneities of conformational dynamics are more pronounced in the vicinity of the TiO_2 surfaces, in harmony with more stretched orientational correlation functions of interfacial PEO. A heterogeneous nature of conformational dynamics was also reported for models of pure (poly)butadiene and PEO melts.[11,19,32] Furthermore, we have found a pronounced discrepancy between even and uneven n, indicating that correlated forward−backward jumps are a very important aspect of polymer dynamics at sufficiently low temperatures both in the presence and absence of solid interfaces, i.e., a Markov process does not apply to the torsional motion. Specifically, the dihedrals have a preferred conformational state at any given time and, after the exit of this state, they tend to return within a very short time interval. At the studied temperatures, the dihedrals remember this state for about 30 conformational transitions so that the conformational states are not sampled according to their statistical weights during large parts of conformational and structural relaxation. For the studied temperatures, this memory effect is hardly affected by solid interfaces.

Acknowledgment. The author thanks the Deutsche Forschungsgemeinschaft (DFG) for funding through Grants VO 905/3-1 and VO 905/3-2.

References and Notes

(1) Jones, R. A. L.; Richards, R. W. *Polymers at Surfaces and Interfaces*; Cambridge University Press: Cambridge, U.K., 1999.
(2) Bansal, A.; Yang, H.; Li, C.; Cho, K.; Benicewicz, B. C.; Kumar, S. K.; Schadler, L. S. *Nat. Mater.* **2005**, *4*, 693.
(3) Rittigstein, P.; Priestley, R. D.; Broadbelt, L. J.; Torkelson, J. M. *Nat. Mater.* **2007**, *6*, 278.
(4) Kropka, J. M.; Pryamitsyn, V.; Ganesan, V. *Phys. Rev. Lett.* **2008**, *101*, 075702.
(5) McKenna, G. B. *Eur. Phys. J. Spec. Top.* **2007**, *141*, 291.
(6) Starr, F. W.; Schroder, T. B.; Glotzer, S. C. *Macromolecules* **2002**, *35*, 4481.
(7) Smith, G. D.; Bedrov, D.; Li, L.; Byutner, O. *J. Chem. Phys.* **2002**, *117*, 9478.
(8) Smith, G. D.; Bedrov, D.; Borodin, O. *Phys. Rev. Lett.* **2003**, *90*, 226103.
(9) Baschnagel, J.; Meyer, H.; Varnik, F.; Metzger, S.; Aichele, M.; Müller, M.; Binder, K. *Interface Science* **2003**, *11*, 159.
(10) Baschnagel, J.; Varnik, F. *J. Phys.: Condens. Matter* **2005**, *17*, R851.
(11) Paul, W.; Smith, G. D. *Rep. Prog. Phys.* **2004**, *67*, 1117.
(12) Borodin, O.; Smith, G. D.; Bandyopadhyaya, R.; Byutner, O. *Macromolecules* **2003**, *36*, 7873.
(13) Kuppa, V.; Foley, T. M. D.; Manias, E. *Eur. Phys. J. E* **2003**, *12*, 159.
(14) Kuppa, V.; Manias, E. *J. Polym. Sci.: Part B: Polym. Phys.* **2005**, *43*, 3460.
(15) Harmandaris, V. A.; Daoulas, K. C.; Mavrantzas, V. G. *Macromolecules* **2005**, *38*, 5796.
(16) Smith, J. S.; Borodin, O.; Smith, G. D.; Kober, E. M. *J. Polym. Sci.: Part B: Polym. Phys.* **2007**, *45*, 1599.
(17) Eslami, H.; Müller-Plathe, F. *J. Phys. Chem. B* **2009**, *113*, 5568.
(18) Vogel, M.; Herbers, C.; Koch, B. *J. Phys. Chem. B* **2008**, *112*, 11217.
(19) Vogel, M. *Macromolecules* **2008**, *41*, 2949.

(20) Chung, S. H.; Wang, Y.; Greenbaum, S. G.; Marcinek, M.; Persi, L.; Croce, F.; Wieczorek, W.; Scrosati, B. *J. Phys.: Condens. Matter* **2001**, *13*, 11763.
(21) Hayamizu, K.; Akiba, E.; Bando, T.; Aihara, Y. *J. Chem. Phys.* **2002**, *117*, 5929.
(22) Singh, T. J.; Bhat, S. V. *J. Power Sources* **2004**, *129*, 280.
(23) Lilley, S. J.; Andreev, Y. G.; Bruce, P. G. *J. Am. Chem. Sci.* **2006**, *128*, 12036.
(24) Zhang, C.; Andreev, Y. G.; Bruce, P. G. *Angew. Chem., Int. Ed.* **2007**, *46*, 2848.
(25) Lindahl, E.; Hess, B.; van der Spoel, D. *J. Mol. Mod.* **2001**, *7*, 306. Berendsen, H. J. C.; van der Spoel, D.; van Drunen, R. *Comput. Phys. Commun.* **1995**, *91*, 43.
(26) Essman, U.; Perela, L.; Berkowitz, M. L.; Darden, T.; Lee, H.; Pedersen, L. G. *J. Chem. Phys.* **1995**, *103*, 8577.
(27) Hess, B.; Bekker, H.; Berendsen, H. J. C.; Fraaije, J. G. E. M. *J. Comput. Chem.* **1997**, *18*, 1463.
(28) Berendsen, H. C. J.; Postma, J. P. M.; DiNola, A.; Haak, J. R. *J. Chem. Phys.* **1984**, *81*, 3684.
(29) Nosé, S. *Mol. Phys.* **1984**, *52*, 255. Hoover, W. G. *Phys. Rev. A* **1985**, *31*, 1695.
(30) Helfand, E.; Wasserman, Z. R.; Weber, T. A. *Macromolecules* **1980**, *13*, 526.
(31) Paul, W.; Smith, G. D.; Yoon, D. Y. *Macromolecules* **1997**, *30*, 7772.
(32) Smith, G. D.; Borodin, O.; Paul, W. *J. Chem. Phys.* **2002**, *117*, 10350.
(33) Elmahdy, M. M.; Chrissopoulou, K.; Afratis, A.; Floudas, G.; Anastasiadis, S. H. *Macromolecules* **2006**, *39*, 5170.
(34) Jin, X.; Zhang, S.; Runt, J. *Polymer* **2002**, *43*, 6247.